Mod Pathol 38 (2025) 100630

MODERN PATHOLOGY

USCAP UNITED STATES AND CANADIAN ACADEMY OF PATHOLOGY
Creating a Better Pathologist

Journal homepage: https://modernpathology.org/

Research Article

Spatial Profiling of Ovarian Clear Cell Carcinoma Reveals Immune-Hot Features

Ya-Ting Tai[a], Wei-Chou Lin[b], Jieru Ye[c], Denis T.-H. Chen[d], Ko-Chen Chen[c], Duncan Y.-T. Wang[c], Tuan Z. Tan[e], Lin-Hung Wei[a], Ruby Y.-J. Huang[c,f,g,*]

[a] *Department of Obstetrics and Gynecology, College of Medicine, National Taiwan University, Taipei, Taiwan;* [b] *Department of Pathology, National Taiwan University Hospital, Taipei, Taiwan;* [c] *School of Medicine, College of Medicine, National Taiwan University, Taipei, Taiwan;* [d] *School of Medicine, College of Medicine, Keele University, Newcastle, United Kingdom;* [e] *Cancer Science Institute of Singapore, National University of Singapore, Center for Translational Medicine, Singapore, Singapore;* [f] *Graduate Institute of Oncology, College of Medicine, National Taiwan University, Taipei, Taiwan;* [g] *Department of Obstetrics and Gynecology, Yong Loo Lin School of Medicine, National University of Singapore, Singapore, Singapore*

ARTICLE INFO

Article history:
Received 25 July 2023
Revised 20 August 2024
Accepted 27 September 2024
Available online 10 October 2024

Keywords:
ovarian cancer
spatial profiling
tumor-infiltrating immune cells
tumor microenvironment

ABSTRACT

Ovarian clear cell carcinoma (OCCC) has a high incidence in Asia, with a frequent occurrence at an early stage, but without sufficient data on molecular stratification for high-risk patients. Recently, immune-hot features have been proposed as indicators of poor prognosis in early stage OCCC. Specific patterns of intratumoral heterogeneity associated with immune-hot features must be defined. NanoString Digital Spatial Profiling technology (Cold spring biotech corp.) was used to decipher the spatial distribution of the 18-plex protein panel. Regions of interest (ROIs) were collected based on the reference hematoxylin and eosin–stained morphology. Areas of illumination (AOIs) were defined according to the ROI segmentation using the fluorescence signals of the visualization markers pan-cytokeratin (PanCK), CD45, or DNA. Unsupervised hierarchical clustering of 595 AOIs from 407 ROIs showed that the PanCK segments expressed different combinations of immune markers, suggestive of immune mimicry. The following 3 immune-hot clusters were identified: granzyme B–high, immune signal-high , and immune-like cells; the following 2 immune-cold clusters were identified: fibronectin-high and immune checkpoint–high cells. In tumor samples at the International Federation of Gynecology and Obstetrics stage IC1/2 experiencing recurrence, there was an increased occurrence of PanCK+ AOIs with immune signal-high and immune-like cell groups in the papillary morphology surrounded by macrophage lineage tumor-infiltrating immune cells (TIIs). In contrast, for tumor samples at the International Federation of Gynecology and Obstetrics stage IC3/II with recurrence, PanCK+ AOIs were prevalent in the fibronectin-high group, particularly in those with a tubulocystic morphology surrounded by lymphoid lineage non-TIIs. Our study on the spatial profiling of early stage OCCC tumors revealed that the immune mimicry of tumor cells, presence of TIIs, and morphologic patterns were associated with recurrence, which switched during tumor progression.

© 2024 THE AUTHORS. Published by Elsevier Inc. on behalf of the United States & Canadian Academy of Pathology. This is an open access article under the CC BY license (http://creativecommons.org/licenses/by/4.0/).

Introduction

In 2023, ovarian cancer was the fifth leading cause of cancer-related mortality among women globally, despite not ranking

* Corresponding author.
E-mail address: rubyhuang@ntu.edu.tw (R.Y.-J. Huang).

0893-3952/© 2024 THE AUTHORS. Published by Elsevier Inc. on behalf of the United States & Canadian Academy of Pathology. This is an open access article under the CC BY license (http://creativecommons.org/licenses/by/4.0/).
https://doi.org/10.1016/j.modpat.2024.100630

among the top 10 newly diagnosed cancers in the population.[1] This indicates the high mortality rate of ovarian cancer compared with its relatively low incidence. Among the various subtypes, epithelial ovarian carcinoma constitutes >90% of the cases and is further categorized into at least 5 subtypes based on histologic and molecular genetic features.[2-4] One such subtype, ovarian clear cell carcinoma (OCCC), is distinguished biologically and clinically.

Biologically, OCCC is characterized by intricate intertumoral and intratumoral heterogeneity. Several studies have focused on its molecular and genetic dimensions,[5,6] focusing on unraveling the mechanisms underpinning OCCC progression to develop tailored treatments. Mutations in key genes associated with OCCC, such as *ARID1A* and *PIK3CA*, are suspected to be early events in the transformation of endometriosis to OCCC.[7,8] Approximately, *ARID1A* mutation accounts for 46% and *PIK3CA* mutation accounts for 43% of OCCC cases, respectively. Previous research conducted in our laboratory has also identified diverse gene expression subtypes in OCCC, featuring mechanisms such as epithelial-mesenchymal transition and immune-related signatures that drive tumor progression and correlate with outcomes.[9,10] Understanding these biological features can help decipher the intertumoral heterogeneity of OCCC and facilitate patient stratification for potential therapeutic interventions.

Clinically, although most OCCC cases are diagnosed at an early stage, metastatic or recurrent OCCC poses significant challenges because of limited therapeutic strategies.[4,11] Therefore, biomarkers are essential for identifying patients at a high risk of recurrence to design tailored novel treatments. The presence of tumor-infiltrating lymphocytes has emerged as a prognostic factor for various solid tumors, including ovarian carcinoma.[12-14] However, the prognostic role of tumor-infiltrating lymphocytes in OCCC and whether tumor-infiltrating lymphocytes can serve as clinical indicators of OCCC recurrence remain unclear.

OCCC also exhibits heterogeneity in terms of its pathologic architecture, comprising the following 3 distinct patterns: papillary, tubulocystic, and solid. Veras et al[15] provided some indirect evidence of the relationship between OCCC morphology and prognosis. Similarly, in clear cell renal cell carcinoma, which shares a similar histologic morphology with OCCC, Cai et al[16] defined 33 phenotypes according to spatial architecture, cytologic features, and the tumor microenvironment (TME) and illustrated their associations with clinical behaviors such as prognosis and drug resistance.

Drawing parallels to clear cell renal cell carcinoma, there is a need to explore the complex morphology of OCCC and its contribution to molecular or genetic heterogeneity. Previous studies have focused on the relationship between OCCC morphology and protein expression using immunohistochemistry.[17,18] However, whether these morphologic features correlate with other molecular signals and serve as predictors of disease outcomes remains unclear. Therefore, it is reasonable to further explore morphologic heterogeneity and molecular intratumoral heterogeneity in OCCC.

Digital spatial profiling (DSP) is a promising method for understanding the spatial distribution of proteins or RNAs within tissues, offering advanced multiplexing and quantification of the markers.[19-21] Furthermore, DSP enables the visualization of tissue morphology, allowing users to define the region of interest (ROI) and detect multiple molecular targets in situ simultaneously without tissue damage.[20,21] In this study, we used DSP technology to capture spatial information on molecular and morphologic heterogeneity, aiming to identify the geospatial correlation between tumor-infiltrating lymphocytes and other immune cells in early stage OCCC tumors. Our objective was to provide new insights into OCCC using state-of-the-art spatial technology to identify potential biomarkers for patient stratification.

Materials and Methods

Clinical Cohort and Data

This institutional review board—approved retrospective cohort study (institutional review board number: 202008022RINB) was conducted at the National Taiwan University Hospital. We reviewed a clinical cohort of 195 patients with stage I or II OCCC.[22] Ten patients (cohort 1) were randomly selected as the pilot cohort to evaluate 18 core protein targets for discovery. For validation, additional 12 patients (cohort 2) were included to evaluate extended 28-plex immuno-oncology proteins. The 2 cohorts were combined as the final study cohort. Patient disease status is outlined in Table 1. No statistically significant differences were observed in the distribution of age, the International Federation of Gynecology and Obstetrics (FIGO) stage, cooccurrence with endometriosis, median follow-up time, recurrence rate, disease-free survival (DFS) time, or mortality between the 2 cohorts. Notably, the median follow-up time of the final cohort was 32.0 months.

In both cohort 1 and cohort 2, all patients underwent adjuvant chemotherapy at the National Taiwan University Hospital following optimal debulking surgery, reflecting a consistent treatment approach. However, there were 2 exceptions in these cohorts. The patient associated with sample 5 was lost to follow-up after undergoing optimal debulking surgery. In addition, the patient linked to sample 15 underwent suboptimal debulking surgery owing to the seeding of multiple tumors at the pelvic side wall (Supplementary Table S1). Supplementary Figure S1 provides a detailed timeline of the disease course and secondary treatment for all the patients with recurrence.

Sample Preparation

Archived formalin-fixed, paraffin-embedded (FFPE) samples were retrieved. Two serial FFPE tissue sections (5 μm) were used for hematoxylin and eosin staining and DSP sample preparation. Each slide was reviewed by an expert pathologist (W.-C.L.) to confirm the diagnosis of OCCC and annotate the distribution of morphologic patterns (papillary, tubulocystic, and solid). Areas of stroma, necrosis, hemorrhage, and damage were avoided. W.-C.L. selected the most representative ROIs from each morphologic area. FFPE tissue sections (5 μm) were baked at 60 °C for 1 hour. Deparaffinization was performed using CitriSolv (Decon labs, Inc) and the sections were sequentially rehydrated in 100% and 95% ethanol, followed by washing with ddH2O. Antigen retrieval was performed by boiling at 121 °C in pH 6 citrate buffer solution for 15 minutes in a pressure cooker. Tissue sections were blocked in blocking buffer for 1 hour at room temperature before incubating with nanoString GeoMx DSP Immune Cell Profiling (NanoString) (a panel of antibodies with UV photocleavable oligonucleotide barcodes), PanCK-Cy3 (1:40), and CD45- Texas Red (1:40) antibodies overnight at 4 °C in the dark. Sections were stained with SYTO13 (NanoString) (1:10) for 15 minutes on the day following fixation in 4% paraformaldehyde.

Digital Spatial Profiling

FFPE samples were incubated with a mixture of visualization markers and DSP probes, which were attached to oligonucleotides using photocleavable linkers. Once scanned using the DSP technology, visualization markers allow users to select ROIs and define areas of illumination (AOIs) based on ROI segmentation using pan-

Table 1
Clinical characteristics of patients.

Variables	Combined	Cohort 1	Cohort 2	*P* value
Patient no.	22	10	12	
Mean age (y), IQR	55.4, 22-72	50.8, 22-64	59.3, 42-72	
FIGO stage, n (%)				0.82[a]
IC1	6 (27.3)	6 (60)	0 (0)	
IC2	4 (18.2)	1 (10)	3 (25)	
IC3	4 (18.2)	1 (10)	3 (25)	
IIA	3 (13.6)	1 (10)	2 (16.7)	
IIB	5 (22.7)	1 (10)	4 (33.3)	
Endometriosis, n (%)	20 (90.9)	9 (90)	11 (91.7)	0.71[b]
Median follow-up time (mo)	32.0 ± 18.6	37.6 ± 17.5	30.8 ± 19.8	0.46[a]
Recurrence, n (%)	8 (36.4)	3 (30)	5 (41.7)	0.45[b]
Median disease-free survival time (mo)	32.2 ± 23.8	29.1 ± 22.9	34.8 ± 25.2	0.59[a]
Death no., n (%)	7 (31.8)	2 (20)	5 (41.7)	0.45[b]

FIGO, International Federation of Gynecology and Obstetrics.
[a] Evaluated using the *t* test.
[b] Evaluated using the Fisher exact test.

cytokeratin (PanCK), CD45, or DNA. The UV light projected by the DSP machine cleaves the linkers in the well-defined AOIs, and the released oligonucleotides are collected with a microcapillary system for further counting using the nCounter system (NanoString). Selected segmented AOIs from each ROI were profiled using nanoString Human Protein Core (NanoString), which consisted of 18 protein targets, including Ki-67, fibronectin (FN), PanCK, cytotoxic T lymphocyte–associated protein 4 (CTLA4), programmed cell death ligand 1 (PD-L1), programmed cell death protein 1 (PD-1), CD20, smooth muscle actin (SMA), granzyme B (GZMB), CD8, β2-globulin, CD45, CD11c, human leukocyte antigen-DR (HLA-DR), CD4, CD3, and CD56. Another panel of 10 immune-ontology proteins was added in cohort 2, including arginase 1 (ARG1), lymphocyte activation gene 3 (LAG3), glucocorticoid-induced TNFR-related protein (GITR), 4-1BB, OX40 ligand, indoleamine 2,3-dioxygenase 1, tim-3, B7-H3, V-domain Ig suppressor of T-cell activation, and stimulator of interferon genes.

Regions of Interest

In cohort 1, 229 ROIs were selected based on their morphology in hematoxylin and eosin staining, with 252 AOIs collected based on their visualization marker segmentations. Among these, 209 AOIs were segmented using PanCK, 41 AOIs were segmented using CD45, and 2 AOIs were segmented using DNA. Twenty-three ROIs were positive for both PanCK and CD45 segments (Fig. 1A). In the 20 ROIs, the PanCK and CD45 segments were intermingled and defined as containing tumor-infiltrating immune cells (TIIs). However, in the 3 ROIs, the PanCK and CD45 segments were geospatially separated, indicating that immune cells surrounded the tumor cells and did not infiltrate them (Fig. 1B). These patients were defined as non-TIIs. Based on the same principle, 178 ROIs with 343 AOIs were selected for cohort 2. A total of 174 AOIs were segmented using PanCK, and 169 AOIs were segmented using CD45. A total of 165 ROIs were positive for both PanCK and CD45 segments, with 65 ROIs containing TIIs and 100 ROIs containing non-TIIs (Fig. 1A).

Data Normalization and Visualization

The readouts from nCounter (version 4.0.0.3) (NanoString) were transferred to GeoMx, QC, and normalized using the built-in data analysis software (version 2.1.0.33) (NanoString). Raw data were first normalized to External RNA Control Consortium spike-in controls. Subsequently, the spike-in normalized data were scaled using the geometric mean of the nuclei counts and using the geometric mean of rabbit immunoglobulin G. The normalized data were log transformed, and the genes and arrays were mean centered using Cluster 3.0 (Michael Eisen, Stanford University).[23] Clustering was also performed using Cluster 3.0, the similarity metric of Pearson correlation, and the tree construction method of centroid linkage. A heatmap of the clustered data was generated using Java Treeview (version 1.1.6r4).[24] Normalized data were extracted and converted into box plots. Statistical significance of the association was assessed using the χ^2 test, whereas the mean difference was assessed using the analysis of variance test.

Survival Analyses

Kaplan–Meier analyses were conducted using GraphPad Prism 10.1.2 (GraphPad Software). Statistical significance of Kaplan–Meier analyses was calculated using the Mantel–Haenszel test. Considering the multivariate of tumor mixture, tumor samples were assigned in a binary fashion to conduct Kaplan–Meier analyses by comparing a certain feature with the rest.

Results

Clustering of Areas of Illumination Revealed PanCK Segments Harboring Various Immune Mimicry Features

The following 2 major clusters were identified from the unsupervised hierarchical clustering of cohort 1 (Fig. 2A): “immune hot” and “immune cold.” These can be further divided into several subclusters according to the conventional shared features of the PanCK+ segments. The “GZMB group” represented epithelial cells exhibiting high signals of PanCK, CD20, and GZMB. The immune signal-high (IH) group featured epithelial cells with robust immune signals and strong expression of myeloid and lymphoid markers. Myeloid signals in this subcluster included CD11c and CD68, whereas lymphoid signals included HLA-DR, CD4, CD3, and CD56. The immune-like (IL) group was characterized by relatively low PanCK expression and coclustered with the CD45+ AOIs. The

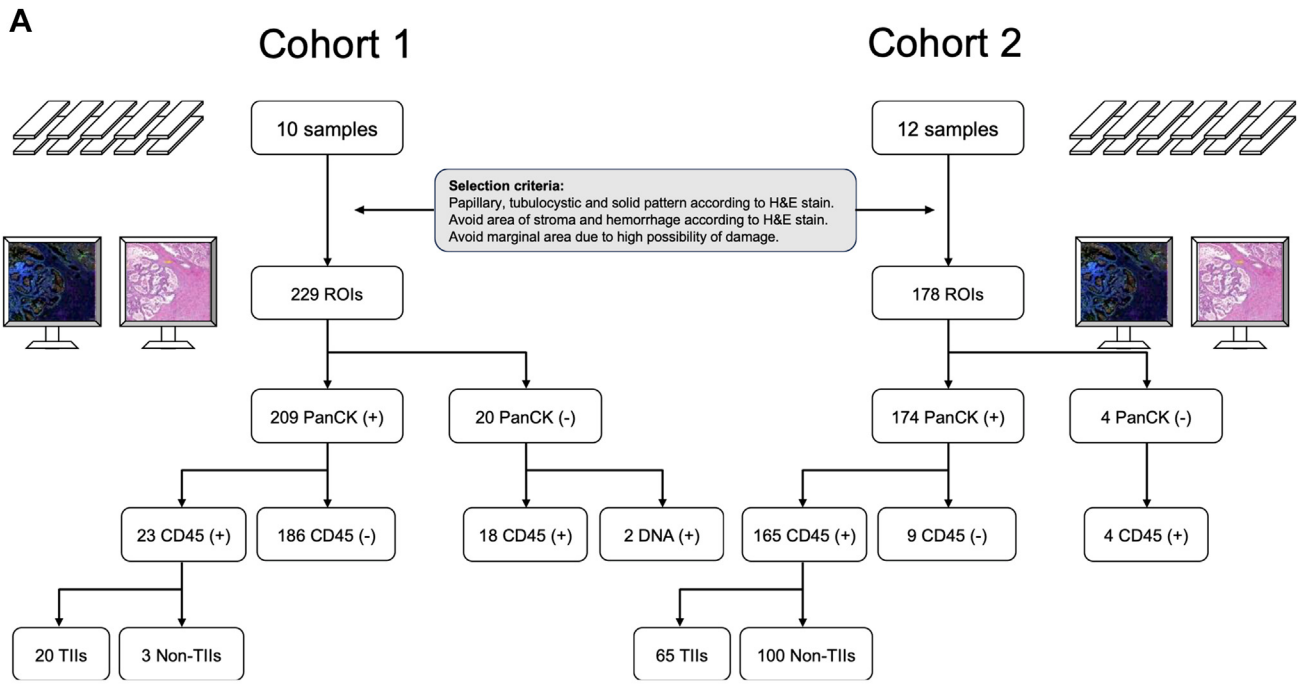

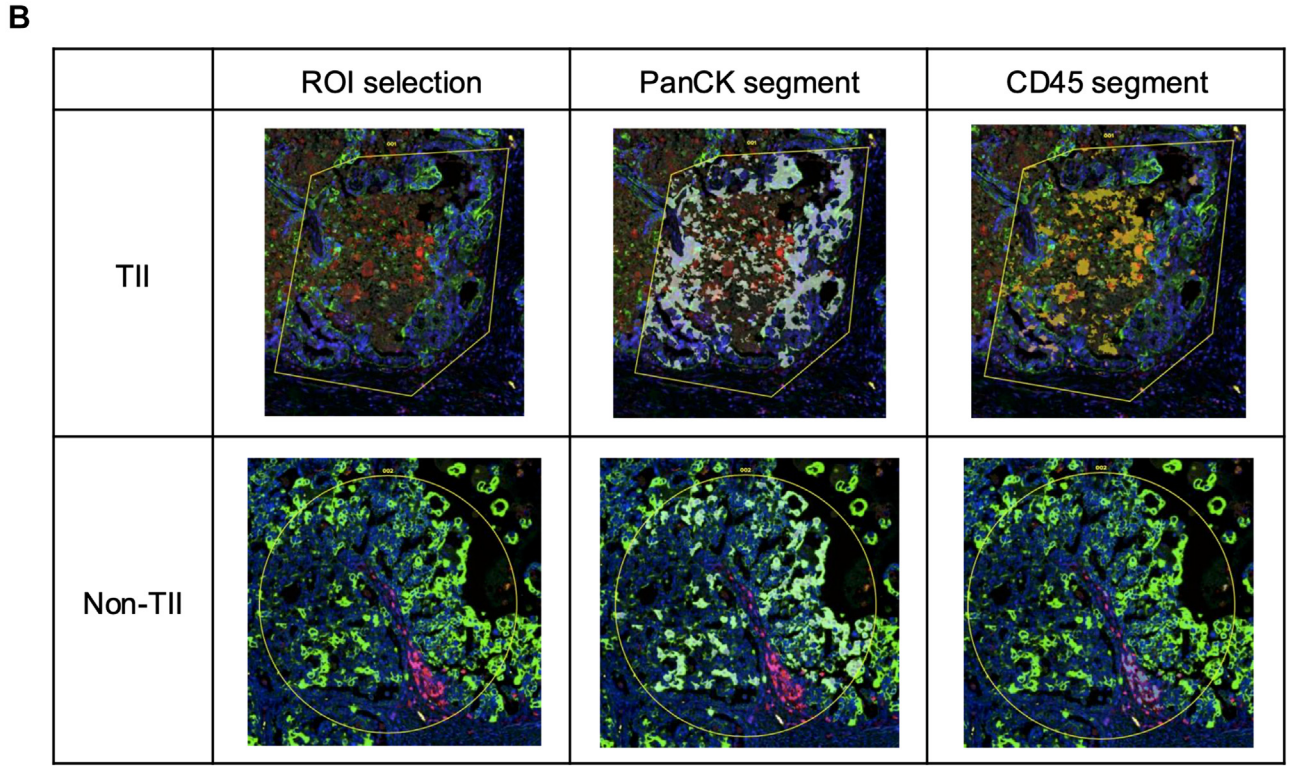

Figure 1.
Region of interest (ROI) selection. (A) The workflow of ROI selection in cohort 1 and cohort 2. (B) Identification of tumor-infiltrating immune cells (TIIs) (upper panel) and non-TIIs (lower panel). Hematoxylin and eosin (H&E)-stained sections were used for morphologic confirmation prior to sample preparation. Images of visualization marker–stained fluorescence of DNA (blue), pan-cytokeratin (PanCK) (green), and CD45 (red) were labeled with the selected ROIs.

FN group displayed epithelial cells with high expression levels of FN, PanCK, and myeloid cell markers, such as CD68. The immune checkpoint (IC) group featured epithelial cells with relatively low expression of PanCK but higher expression of IC signals, CTLA4, and PD-1 (Fig. 2C). These spatially resolved PanCK+ segments exhibited different combinations of immune markers, suggesting

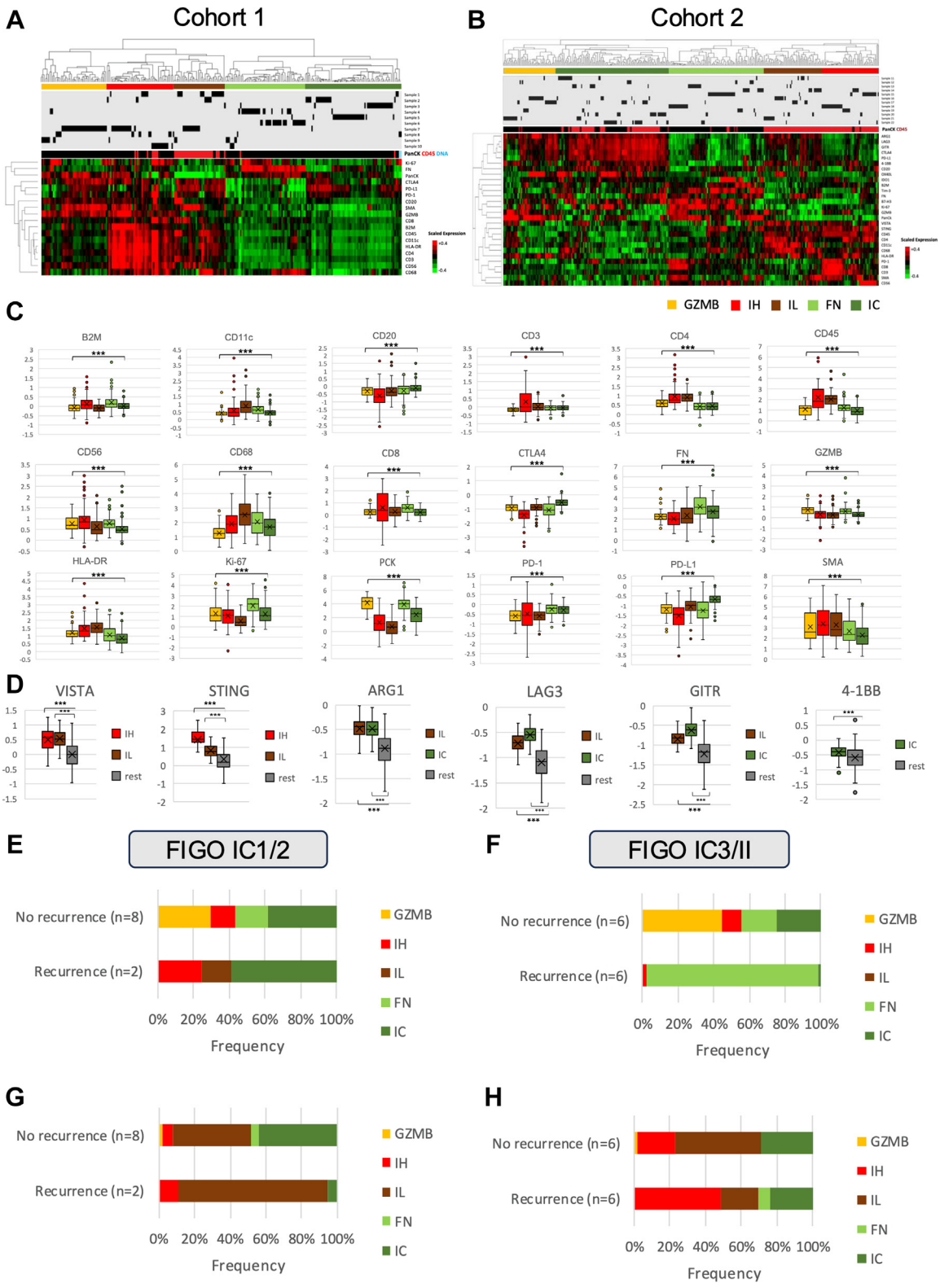

Figure 2.

Clustering of areas of illumination (AOIs) and association with tumor recurrence. (A) Unsupervised hierarchical clustering of 18-plex protein expression data for cohort 1. PanCK+ segments (black stripes), CD45+ segments (red stripes), and DNA-positive segments (blue stripes) among all analyzed AOIs. From left to right: granzyme B (GZMB) (orange), immune signal-high (IH) (red), immune-like (IL) (brown), fibronectin (FN) (light green), and immune checkpoint (IC) (dark green) groups. Each black stripe in the gray panels indicates the AOI for a specific sample. The heatmap represents the normalized intensity of 18-plex protein expression. (B) Unsupervised hierarchical clustering of 28-plex protein expression data in cohort 2 (GZMB, orange; IH, red; IL, brown; FN, light green; IC, dark green). (C) Intensity of the normalized protein signals from 5 clusters of PanCK+ segments (GZMB, orange; IH, red; IL, brown; FN, light green; IC, dark green), with statistical significance determined using 1-way analysis of variance; $^{**}P < .01$, $^{***}P < .001$. Y axis: numerical values of normalized protein expression levels (extracted from the heatmap). (D) Intensity of the normalized immuno-oncological protein signals from selected

distinctive immune mimicry features. We noticed that the AOIs from different patients contributed to each cluster, indicating the existence of intertumoral heterogeneity (Supplementary Table S1). The PanCK+ segments in cohort 2 showed similar 5 clusters in unsupervised hierarchical clustering (Fig. 2B). However, the GZMB group in cohort 2 coclustered with the immune-cold cluster. To maintain consistency, we would refer to each cluster by the name assigned to cohort 1.

The CD45+ AOIs from cohort 1 displayed distinct groupings within specific clusters. Notably, the GZMB group did not contain CD45+ segments. Most CD45+ AOIs were grouped into IH and IL groups. CD45+ AOIs in the IH group expressed significantly strong immune-related signals, including CD45, CD11c, HLA-DR, CD4, CD3, and CD56, indicating the presence of antigen-presenting cells, natural killer (NK) cells, and T helper cells. In contrast, CD45+ AOIs in the IL group expressed relatively robust immunosuppressive signals, including CTLA4, PD-L1, and PD-1. One CD45+ AOI was identified in the FN group, exhibiting cold immune signals, whereas another CD45+ AOI in the IC group displayed high CTLA4 and PD-L1 signals. CD45+ segments in cohort 2 demonstrated characteristics similar to those in cohort 1 (Fig. 2B). The integration of 10 additional immune-ontology protein markers in cohort 2 provided a more comprehensive insight into the immune cell landscape. Both the IH and the IL group CD45+ AOIs showed high signals of V-domain Ig suppressor of T-cell activation and stimulator of interferon genes, suggesting the potential suppression of T-cell activation and interferon response. The IL group CD45+ AOIs also showed relatively high signals for CD68, ARG1, LAG3, and GITR, indicating the presence of immunosuppressive macrophage lineage immune cells. The IC group CD45+ AOIs showed significantly high signals for ARG1, LAG3, GITR, and 4-1BB, in addition to IC markers, further highlighting the intricate immune landscape within these clusters (Fig. 2D).

The Presence of PanCK Segments Within Immune Mimicry Clusters was Associated With Ovarian Clear Cell Carcinoma Recurrence

Our previous study revealed an immune switch from "immune cold" to "immune hot" during the progression of early stage OCCC.[22] Building on this, we pooled normalized data from cohorts 1 and 2 to further investigate the molecular and morphologic characteristics of FIGO stages IC1/2 and IC3/II.

Different cluster distribution of PanCK segments in OCCC recurrence was noted in different stages. In both stages, PanCK+ segments in the GZMB group were exclusively present in patients without recurrence (Fig. 2E, F and Supplementary Fig. S2). In patients with IC1/2 with recurrence, PanCK+ segments appeared exclusively in the IL group. The PanCK+ segments in certain clusters showed paradoxical distribution frequencies between IC1/2 and IC3/II. In IH and IC groups, PanCK+ segments exhibited a higher frequency in IC1/2 with recurrence (24.1% in recurrence vs 13.9% in no recurrence; 58.6% in recurrence vs 38.2% in no recurrence), whereas a lower frequency in IC3/II with recurrence (2.2% in recurrence vs 10.9% in no recurrence; 1.1% in recurrence vs 33.3% in no recurrence). FN group PanCK+ segments were exclusively observed in patients with IC1/2 with no recurrence but exhibited a significantly higher frequency in patients with IC3/II with recurrence (96.6% in recurrence vs 19.6% in no recurrence). These findings suggest that PanCK+ tumor cells undergo a switch in immune features from the IH/IL/IC group to the FN group as OCCC progresses from IC1/2 to IC3/II, and that this switch is associated with recurrence.

Different cluster distribution of CD45 segments in OCCC recurrence was also noted in different stages. In IC1/2, the IL group showed a significantly higher frequency of recurrence (84.2% in recurrence vs 44.2% in no recurrence), whereas the IC group exhibited a lower frequency of recurrence (5.3% in recurrence vs 44.2% in no recurrence) (Fig. 2G and Supplementary Fig. S2). In contrast, in IC3/II, the IH group showed a higher frequency in patients with recurrence (48.2% in recurrence vs 21.4% in no recurrence), whereas the IL group displayed a lower frequency in patients with recurrence (21.7% in recurrence vs 32.4% in no recurrence) (Fig. 2H and Supplementary Fig. S2). These findings suggest that CD45+ immune cells undergo a switch in immune features during OCCC tumor progression, transitioning from the IL to the IH group.

The Presence of Tumor-Infiltrating Immune Cells was Associated With Ovarian Clear Cell Carcinoma Recurrence

We further explored the geospatial relationship between tumor cells and immune cells (TIIs vs non-TIIs) and its association with patient outcomes. TIIs had a higher frequency in PanCK+ segments from tumor samples of IC1/2 patients with recurrence (62.1% in recurrence vs 2.3% in no recurrence). Interestingly, non-TIIs were absent in IC1/2 patients with recurrence (0% in recurrence vs 20.2% in no recurrence). The frequency of PanCK+ segments without CD45 cosegmentation was also reduced (37.9% in recurrence vs 77.5% in no recurrence) (Fig. 3A, Supplementary Fig. S2, and Supplementary Tables S1-S3). In contrast, in patients with IC3/II with recurrence, the TIIs did not show a significant difference. Instead, there was a higher frequency of non-TII occurrence (61.8% in recurrence vs 37.0% in no recurrence) (Fig. 3B, Supplementary Fig. S2, and Supplementary Tables S1-S3). This suggests a shift in the tumor infiltration status of immune cells as the disease progresses.

Next, we investigated the neighborhood context between tumor cell clusters and immune cells. We asked whether there were specific tumor cell clusters that were more enriched or excluded from the TIIs. In IC1/2, TIIs appeared with a high frequency in the IH group PanCK+ segments (31.8%, χ^2: $P = 2.3E-02$), a low frequency in the GZMB group PanCK+ segments (4.5%, χ^2: $P = 1.8E-02$), and no occurrence in the FN group PanCK+ segments (0%, χ^2: $P = 3.1E-02$). The IL group was exclusively found in the PanCK+ segments, with TIIs in IC1/2 (Fig. 3C). In IC3/II, TIIs showed no significant difference in cluster distribution among the PanCK+ segments. However, non-TIIs showed a relatively high frequency in the FN PanCK+ segments (65.2%, χ^2: $P = 3.9E-02$). PanCK+ segments with no CD45 cosegmentation showed a higher frequency in the IH group (26.9%, χ^2: $P = 1.7E-17$) and the GZMB group (38.5%, χ^2: $P = 4.6E-02$), with a lower frequency in the FN group (34.6%, χ^2: $P = 1.1E-02$) and 0 occurrence in the IC group. At

clusters of PanCK+ segments (GZMB, orange; IH, red; IL, brown; FN, light green; IC, dark green), with statistical significance determined using 1-way analysis of variance; $^{**}P < .01$, $^{***}P < .001$. Y axis: numerical values of normalized protein expression levels (extracted from the heatmap). (E, F) The proportion of PanCK+ segments belonging to different subclusters (GZMB, orange; IH, red; IL, brown; FN, light green; IC, dark green) in tumor samples with or without recurrence in International Federation of Gynecology and Obstetrics stages IC1/2 and IC3/II, respectively. (F, G) The proportion of CD45+ segments belonging to different subclusters (GZMB, orange; IH, red; IL, brown; FN, light green; IC, dark green) in tumor samples with or without recurrence in International Federation of Gynecology and Obstetrics stages IC1/2 and IC3/II, respectively. STING, stimulator of interferon genes; VISTA, V-domain Ig suppressor of T-cell activation.

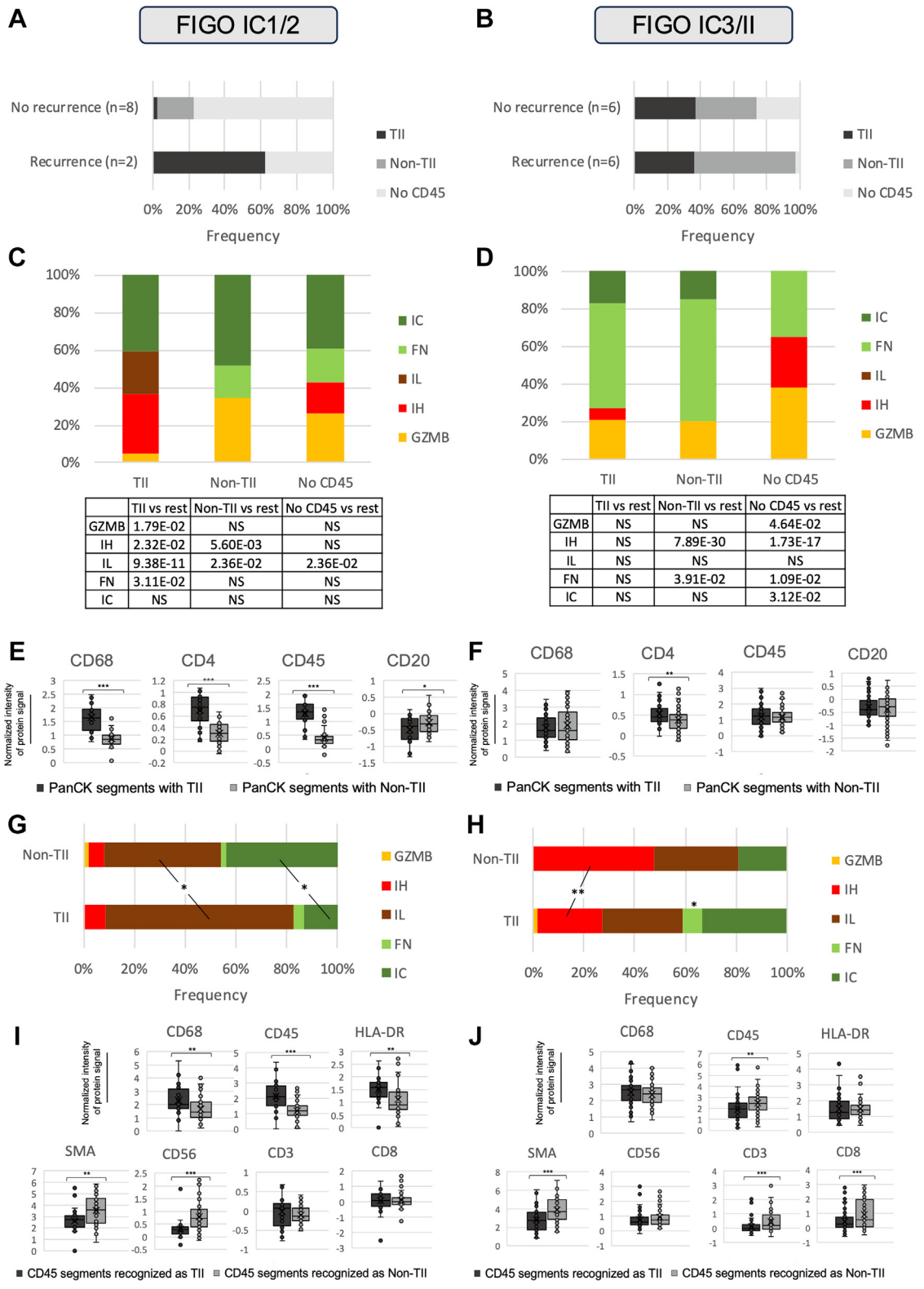

	TII vs rest	Non-TII vs rest	No CD45 vs rest
GZMB	1.79E-02	NS	NS
IH	2.32E-02	5.60E-03	NS
IL	9.38E-11	2.36E-02	2.36E-02
FN	3.11E-02	NS	NS
IC	NS	NS	NS

	TII vs rest	Non-TII vs rest	No CD45 vs rest
GZMB	NS	NS	4.64E-02
IH	NS	7.89E-30	1.73E-17
IL	NS	NS	NS
FN	NS	3.91E-02	1.09E-02
IC	NS	NS	3.12E-02

Figure 3.

The characteristics of tumor-infiltrating immune cells (TIIs) and the surrounding tumor microenvironment. (A, B) The proportion of PanCK+ segments containing TIIs (iron), non-TIIs (dark gray), and no CD45 cosegmentation (light gray) in tumor samples with or without recurrence in International Federation of Gynecology and Obstetrics (FIGO) stages IC1/2 and IC3/II, respectively. (C, D) The proportion of PanCK+ segments belonging to different subclusters (granzyme B [GZMB], orange; immune signal high [IH], red; immune like [IL], brown; fibronectin [FN], light green; immune checkpoint [IC], dark green) in samples with TIIs, non-TIIs, and no CD45 cosegmentation in FIGO stages IC1/2 and IC3/II, respectively. This table shows the results of the χ^2 test. (E, F) Intensity of the normalized protein signals from PanCK+ segments containing TIIs (iron) and non-TIIs (dark gray) in FIGO stages IC1/2 and IC3/II, respectively. Statistical significance was determined using 1-way analysis of variance; $^{**}P < .01$, $^{***}P < .001$. Y axis: numerical values of normalized protein expression levels (extracted from the heatmap). (G, H) The proportion of different CD45 segment subclusters (GZMB, orange; IH, red; IL, brown; FN, light green; IC, dark

both the stages, PanCK+ segments with non-TIIs were not observed in the IH group. These data further corroborate the association between OCCC recurrence and the presence of TIIs/non-TIIs. OCCC recurrence was associated with IH/IL group PanCK+ segments with TIIs in IC1/2 and FN group PanCK+ segments with non-TIIs in IC3/II. In summary, tumor cells with GZMB features are more likely to exclude TIIs. Tumor cells with IH features are more likely to attract myeloid and lymphoid lineages of infiltrating immune cells with high CD45, CD3, and CD8 expression. Tumor cells with IL features would more likely attract immune cells with low expression of immune signals.

Furthermore, we compared the protein expression between PanCK+ segments with TIIs and those with non-TIIs. In IC1/2, PanCK+ segments with TIIs showed elevated expression of CD68, CD45, and CD4, whereas those with non-TIIs showed higher expression of CD20 (Fig. 3E and Supplementary Fig. S3). However, as OCCC progressed to IC3/II, there were minimal significant differences in the immune signals between PanCK+ segments with TIIs and those with non-TIIs (Fig, 3F and Supplementary Fig. S3). Overall, all immune signals from the PanCK+ segments with TIIs and non-TIIs in IC3/II were expressed at levels similar to those from the PanCK+ segments with TIIs in IC1/2 (Fig. 3E, F and Supplementary Fig. S3). This indicated a shift in protein signal expression in tumor cells harboring immune mimicry during the progression of OCCC.

A notable distinction was observed in the cluster distribution of CD45+ segments between TIIs and non-TIIs (Fig. 3G, H). Next, we explored the differences between the immune features of TIIs and non-TIIs. In IC1/2, TIIs showed a higher frequency in IL group CD45+ segments (73.9% in TIIs vs 45.8% in non-TIIs, χ^2: $P = 2.6E-02$), whereas non-TIIs showed a higher frequency in IC group CD45+ segments (26.1% in TIIs vs 43.8% in non-TIIs, χ^2: $P = 1.0E-02$). In IC3/II, TIIs showed a higher frequency in the FN group CD45+ segments (7.6% in TIIs vs 0% in non-TIIs, χ^2: $P = 1.7E-02$), whereas non-TIIs showed a lower frequency in the IL group CD45+ segments (25.8% in TIIs vs 47.9% in non-TIIs, χ^2: $P = 6.9E-03$). A switch in immune cell clusters was observed during OCCC progression. TIIs were switched from IL to FN group CD45+ segments, and non-TIIs were switched from IC to IL group CD45+ segments.

TII and non-TII CD45+ AOIs also showed different immune protein expression signals, suggesting distinct lineages. For IC1/2, TII CD45+ AOIs showed higher expression of CD68, CD45, and HLA-DR, whereas non-TIIs showed higher expression of CD56, SMA, FN, and PanCK (Fig. 3I and Supplementary Fig. S4). However, in IC3/II, both TIIs and non-TIIs demonstrated equally high expression levels of CD68, CD45, and HLA-DR, as observed in the TIIs in IC1/2. In IC3/II, TII CD45+ AOIs showed higher expression levels of CTLA4, PanCK, and Ki-67, whereas non-TIIs showed higher expression of CD3 and CD8 (Fig. 3J and Supplementary Fig. S4). This indicates that TIIs in IC1/2 may be more enriched in the macrophage lineage. In contrast, non-TIIs in IC1/2 appeared to be of the myeloid lineage, which changed to the lymphoid lineage in IC3/II.

Cluster Mixture of PanCK+ Segments and the Presence of Tumor-Infiltrating Immune Cells

Significant inter- and intratumoral heterogeneity was observed in the number of different clusters within the cluster mixture, based on the annotations of the PanCK+ segments (Supplementary Figs. S2 and S5A). Eighteen tumors (81.8%) exhibited heterogeneity in the cluster mixture of PanCK+ segments, with 9 tumors (40.9%) displaying a mix of 2 clusters and another 9 tumors (40.9%) displaying a mix of 3 clusters. The 2-cluster and 3-cluster heterogeneous tumors showed a combination of immune-cold and immune-hot clusters without a significant mixture pattern. Among these heterogeneous tumors, TIIs were identified in 12 tumors (66.7%) adjacent to the PanCK+ segments without specific cluster patterns (Supplementary Figs. S2 and S5A). All 2-cluster tumors were characterized based on the presence of TIIs ($P = .046$). In addition, there was no significant difference in the number of cluster mixtures between tumors from patients with or without recurrence (Supplementary Fig. S5B). The remaining 4 tumors (18.2%) showed high homogeneity of PanCK+ segments in the presence of a single cluster of immune-cold groups. Three of them were in IC3/II, comprising the FN group PanCK+ segments, and were associated with recurrence ($P = .046$). Only 1 tumor showed the presence of TIIs within the FN group PanCK+ segments (Supplementary Figs. S2 and S5A). In summary, the number of cluster mixtures did not correlate strongly with the presence of TIIs or OCCC recurrence. This was due to the specific nature of the cluster mixture, such as the presence of the GZMB cluster, which seemed to determine the occurrence of TIIs.

Intratumoral Heterogeneity of Morphology is Associated With Tumor-Infiltrating Immune Cell Frequency and Cluster Features

There were various degrees of morphologic heterogeneity among different tumors and within each tumor (Supplementary Figs. S2 and S6A). In IC1/2 tumors with recurrence, a higher frequency of papillary patterns (62.1% in recurrence vs 21.4% in no recurrence) and a lower frequency of tubulocystic patterns (6.9% in recurrence vs 42.2% in no recurrence) were observed than in those without recurrence (Fig. 4A). In contrast, IC3/II tumor samples with recurrence showed a higher frequency of tubulocystic patterns (35.2% in recurrence vs 21.3% in no recurrence) (Fig. 4B).

We observed an association between tumor morphology and the TME of the clusters (Fig. 4C, D and Supplementary Table S4). Certain morphologies showed a switch in the predominant PanCK+ segment clusters during OCCC progression. ROIs with a papillary pattern in IC1/2 showed a high frequency of IH PanCK+ segments (29.2%, χ^2: $P = 2.3E-03$) and a low frequency of GZMB and FN PanCK+ segments (14.6%, χ^2: $P = 5.0E-02$; 0%, χ^2 test: $P = 5.7E-04$). However, in IC3/II, ROIs with a papillary pattern showed a high frequency of IC PanCK+ segments (32.7%, χ^2 test: $P = 2.0E-07$) but a relatively low frequency of FN PanCK+ segments (40.4%, χ^2test: $P = 3.2E-03$). ROIs with a tubulocystic pattern in IC1/2 showed a high frequency of GZMB PanCK+ segments (34.7%, χ^2 test: $P = 2.1E-02$) and a low frequency of IC PanCK+ segments (25.0%, χ^2 test: $P = 5.4E-04$). However, there was no significant difference in the cluster distribution of IC13/II tubulocystic ROIs. ROIs with a solid pattern in IC1/2 showed a relatively high frequency of FN PanCK+ segments (22.0%, χ^2 test: $P = 4.9E-02$) and a significantly low frequency of IH PanCK+ segments (2.4%, χ^2

green) in the immune cells were classified as TIIs and non-TIIs in FIGO stages IC1/2 and IC3/II, respectively. (I, J) Intensity of the normalized protein signals from CD45+ segments of TIIs (iron) and non-TIIs (dark gray) in FIGO stages IC1/2 and IC3/II, respectively. Statistical significance was determined using 1-way analysis of variance; $^{**}P < .01$, $^{***}P < .001$. Y axis: numerical values of normalized protein expression levels (extracted from the heatmap). HLA-DR, human leukocyte antigen-DR; NS, no significance; PanCK, pan-cytokeratin; SMA, smooth muscle actin.

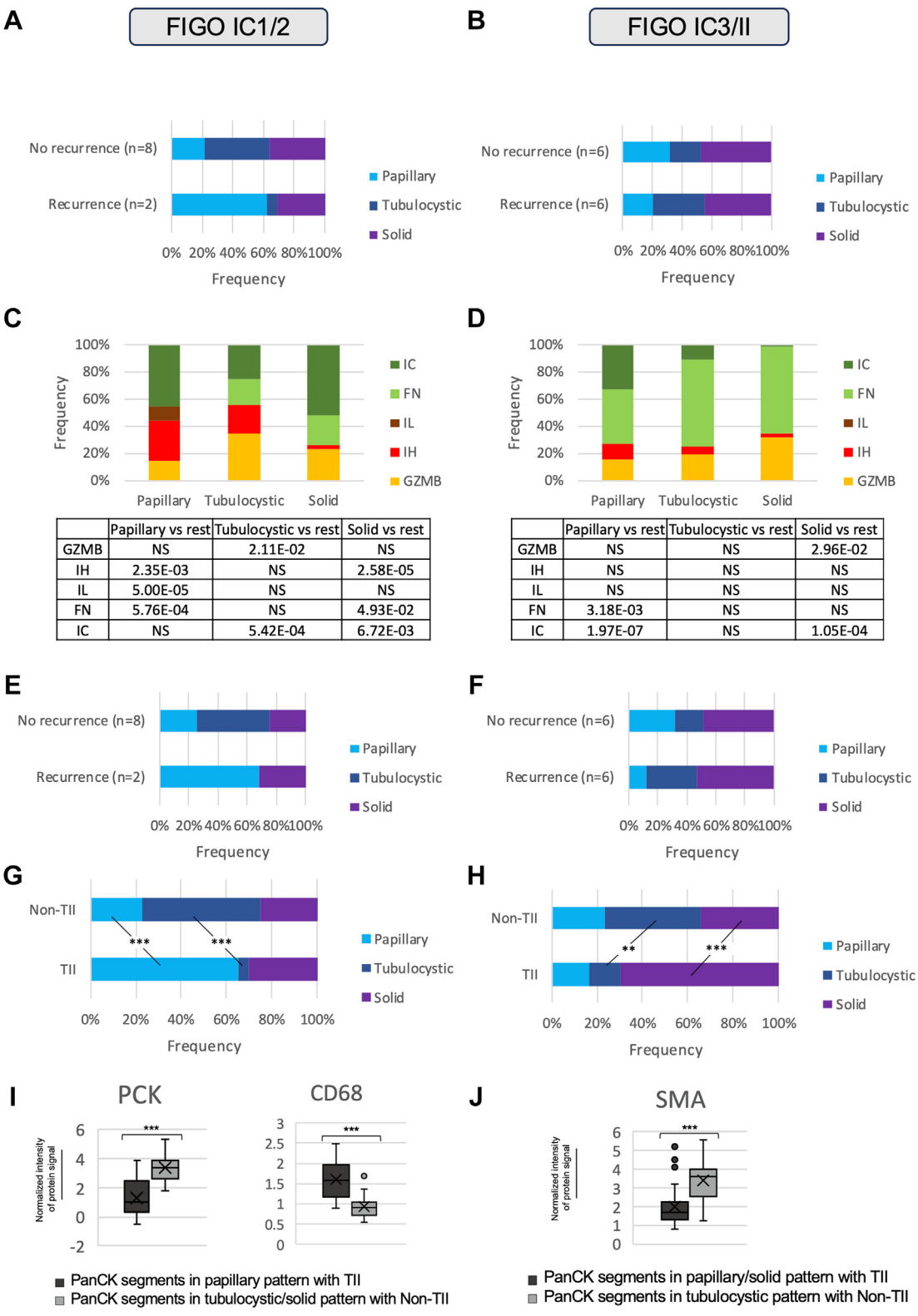

	Papillary vs rest	Tubulocystic vs rest	Solid vs rest
GZMB	NS	2.11E-02	NS
IH	2.35E-03	NS	2.58E-05
IL	5.00E-05	NS	NS
FN	5.76E-04	NS	4.93E-02
IC	NS	5.42E-04	6.72E-03

	Papillary vs rest	Tubulocystic vs rest	Solid vs rest
GZMB	NS	NS	2.96E-02
IH	NS	NS	NS
IL	NS	NS	NS
FN	3.18E-03	NS	NS
IC	1.97E-07	NS	1.05E-04

Figure 4.

Tumor morphology and association with tumor recurrence and tumor-infiltrating immune cells (TIIs). (A, B) The proportion of PanCK+ segments identified as papillary patterns (light blue), tubulocystic patterns (dark blue), and solid patterns (purple) in samples with or without recurrence in International Federation of Gynecology and Obstetrics (FIGO) stages IC1/2 and IC3/II, respectively. (C, D) The proportion of PanCK+ segments belonging to different subclusters (granzyme B [GZMB], orange; immune signal high [IH], red; immune like [IL], brown; fibronectin [FN], light green; immune checkpoint [IC], dark green) in different morphologic patterns in FIGO stages IC1/2 and IC3/II, respectively. This table shows the results of the χ^2 test. (E, F) The proportion of CD45+ segments identified as different morphologic patterns (papillary, light blue; tubulocystic, dark blue; solid, purple) in samples with or without recurrence in FIGO stages IC1/2 and IC3/II, respectively. (G, H) The proportion of CD45+ segments identified as having different morphologic patterns (papillary, light blue; tubulocystic, dark blue; solid, purple) in samples with TIIs and non-TIIs in FIGO stages IC1/2 and IC3/II, respectively. (I, J) Intensity of the

test: $P = 2.6E-05$). In IC13/II, ROIs with a solid pattern showed a high frequency of GZMB PanCK+ segments (31.5%, χ^2 test: $P = 3.0E-02$), but a low frequency of IC PanCK+ segments (1.4%, χ^2 test: $P = 1.1E-04$). In addition, the IL PanCK+ segments were exclusive to ROIs with a papillary pattern in IC1/2. In summary, the ROIs with different morphologic patterns showed changes in the predominant clusters of PanCK+ segments. Papillary ROIs switched from the IH/IL group to the IC group, tubulocystic ROIs switched from the GZMB group to nonspecific predominant clusters, and solid ROIs switched from the FN group to the GZMB group. These findings corroborated the significant exclusiveness observed between recurrences and clusters (Fig. 2C), implying that morphologic heterogeneity could serve as a prognostic indicator in OCCC.

The expression of 18-plex protein signals among the different morphologies was further explored (Supplementary Fig. S6B). Conventionally, PanCK+ segments of either morphology show elevated expression of PanCK and FN as the disease progresses. PanCK+ segments in the tubulocystic pattern showed significantly higher SMA expression than those in the other 2 patterns in both IC1/2 and IC3/II. Specifically, as OCCC progressed, PanCK+ segments in papillary and tubulocystic patterns showed higher CD8 expression. PanCK+ segments in the solid pattern showed lower expression of CTLA4, PD-L1, PD-1, CD3, and CD8, despite the elevation of CD45.

Inter- and intratumoral heterogeneity in the morphology of CD45+ AOIs was also observed (Supplementary Fig. S2 and Supplementary Table S5). In IC1/2, immune cells had a higher frequency within papillary ROIs in tumor samples with recurrence (68.4% in recurrence vs 25.0% in no recurrence), whereas those within tubulocystic ROIs occurred only in tumor samples without recurrence (Fig. 4E). In IC3/II, immune cells showed a higher frequency within papillary ROIs in tumor samples without recurrence (12.0% in recurrence vs 32.1% in no recurrence) (Fig. 4F). This prompted us to examine the correlation between TIIs and morphologic patterns (Supplementary Table S5). In IC1/2, TII CD45+ segments showed a higher frequency of papillary patterns (65.2%, χ^2 test: $P = 5.4E-04$). Non-TII CD45+ segments showed a higher frequency of tubulocystic patterns (4.3%, χ^2 test: $P = 9.3E-05$) (Fig. 4G). In IC3/II, TII CD45+ segments showed a higher frequency in the solid pattern (51.7%, χ^2 test: $P = 2.6E-06$) (Fig. 4H). Immune cells within the tubulocystic pattern were almost exclusively non-TIIs in both the IC1/2 and IC3/II groups (96.2%, χ^2 test: $P = 1.3E-03$; 77.5%, χ^2 test: $P = 4.6E-04$) (Fig. 4G, H). These data clearly demonstrate a significant correlation between OCCC recurrence in IC1/2 and the presence of CD68+ TIIs within the papillary morphology of PanCK+ segments harboring immune-hot cluster features. In IC3/II, OCCC recurrence was associated with the presence of SMA-high non-TIIs around the tubulocystic morphology of the PanCK+ segments featuring a high FN signal (Fig. 4I, J).

Survival Analysis Confirms the Association Between Specific Features and Outcomes in Early Stage Ovarian Clear Cell Carcinoma

Our study highlighted significant changes in specific features associated with early stage OCCC recurrence during tumor progression from FIGO stage IC1/2 to IC3/II (Fig. 5A). We then conducted the following 3 distinct analyses to examine the potential impact of the features on the outcome: first, univariate analysis to confirm the effect of each individual feature on DFS within each tumor sample (Tables 2 and 3); second, Kaplan–Meier analysis for coexisting features to assess the impact of 2 coexisting features on DFS within each tumor sample; third, Kaplan–Meier analysis within each ROI to further validate the effect of coexisting features on DFS.

From the univariate analysis, we found that patients with OCCC in both FIGO stage IC1/2 and IC3/II with GZMB group tumor cells have higher 2-year DFS rates (hazard ratio [HR] = 0.10; $P = .0012$), whereas patients with OCCC with IH group immune cells have lower 2-year DFS rates (HR = 6.16; $P = .0029$). In FIGO stage IC3/II, patients with OCCC with IC group immune cells have higher 2-year DFS rates (HR = 0.13; $P = .011$) (Fig. 5B).

We further analyzed the coexisting features within 1 tumor sample that could have an impact on prognosis. In both FIGO stage IC1/2 and IC3/II, OCCC tumors with a tubulocystic or solid pattern but without any CD45 segments have higher 2-year DFS rates (HR = 0.20, $P = .031$; HR = 0.21, $P = .048$). OCCC tumors with IH group tumor cells and TIIs have lower 2-year DFS rates (HR = 37.43; $P = .0010$). In FIGO stage IC1/2, OCCC tumors with IH group tumor cells and a papillary pattern have lower 2-year DFS rates (HR = 47.47; $P = .017$) (Fig. 5C).

We then explored the specific coexisting feature within 1 ROI associated with prognosis. In FIGO stage IC1/2, OCCC tumors with ROIs in a papillary pattern and TIIs would have lower 2-year DFS rates (HR = 47.47; $P = .017$), and OCCC tumors with ROIs with FN group tumor cells and non-TIIs would also have lower 2-year DFS rates (HR = 5.84; $P = .034$) (Fig. 5D).

Discussion

Immune-related subtypes have been shown to correlate with patient outcomes in OCCC.[9,22,25] These studies were based on the bulk analysis of tumor samples and thus provided a perspective of intertumoral heterogeneity in OCCC. In the present study using DSP technology, we explored the intratumoral heterogeneity of 22 OCCC tumors and analyzed the expression patterns of molecular signals in relation to geospatial context and pathologic morphology. We identified 5 clusters of OCCC cells with immune mimicry using a spatially resolved technique that provided clear compartmentalization between tumor and immune cells. Immune mimicry in tumor cells has been proposed as a mechanism of immune evasion,[26-28] and Gao et al[29] demonstrated that various types of immune mimicry in tumor cells could lead to different clinical outcomes. Three types of immune-hot features indicative of immune mimicry of tumor cells in FIGO stage IC1/2 were observed. OCCC with GZMB group epithelial cells had a favorable prognosis, in which the tumor cells featured high levels of GZMB and CD20. This is consistent with previous studies suggesting that tumor-infiltrating CD20+ B cells correlate with a favorable prognosis in non–small cell lung, breast, cervical, and ovarian cancer.[30-33] Interestingly, this group of epithelial cells expressing high levels of GZMB and CD56 showed low levels of CD4 and CD8, which indicated the mimicry of NK cells instead of T cells. Furthermore, non-TIIs with high levels of SMA were observed at higher frequencies in this group of epithelial cells. In summary, we hypothesized that the NK cell/B cell mimicry of tumor cells with

normalized protein signals from PanCK+ segments with different morphologies with TIIs (iron) and non-TIIs (dark gray), with statistical significance determined using 1-way analysis of variance; $^{**}P < .01$, $^{***}P < .001$. Y axis: numerical values of normalized protein expression levels (extracted from the heatmap). NS, no significance; PanCK, pan-cytokeratin; SMA, smooth muscle actin.

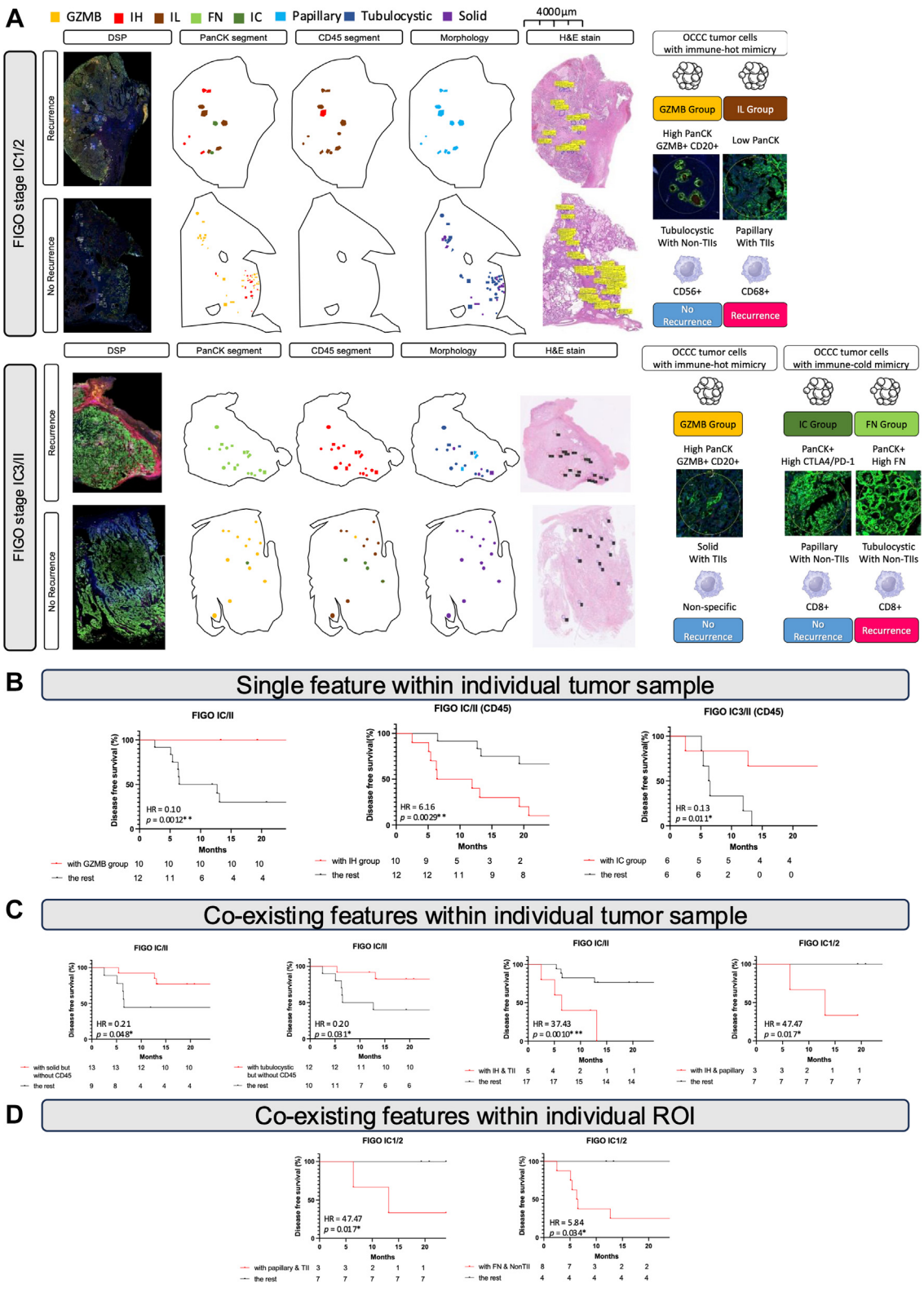

Figure 5.

Specific features associated with early-stage ovarian clear cell carcinoma (OCCC) prognosis. (A) For OCCC in International Federation of Gynecology and Obstetrics (FIGO) stage IC1/2, immune-like (IL) group PanCK+ segments with CD68+ tumor-infiltrating immune cells (TIIs) and papillary patterns were associated with recurrence; granzyme B (GZMB) group PanCK+ segments with CD56+ non-TIIs and tubulocystic patterns were associated with no recurrence. For OCCC in FIGO stage IC3/II, PanCK+ segments with CD8+ non-TIIs and tubulocystic patterns in the fibronectin (FN) group were associated with recurrence; PanCK+ segments with nonspecific TIIs and solid patterns in the GZMB group, and PanCK+ segments with CD8+ non-TIIs and papillary patterns in the immune checkpoint (IC) group were associated with no recurrence. (B) The 2-year disease-free survival rate of patients with OCCC with specific single features vs the rest, GZMB group tumor cells in FIGO stage IC/II, immune signal-high (IH) group immune cells in FIGO stage IC/II, and IC group immune cells in FIGO stage IC3/II, respectively. (C) The 2-year disease-free survival rate of patients with OCCC with specific coexisting features within individual tumor

coexisting immune cells contributes to a better TME and leads to a favorable prognosis. In contrast, OCCC with IH epithelial cells may have a poorer prognosis, in which tumor cells are prone to attract TIIs with high levels of CD45. The immune signals in this group of tumor cells showed nonspecific immune mimicry of the lineages. OCCC with IL epithelial cells has an unfavorable prognosis, in which tumor cells featuring high levels of CTLA4 attract TIIs with high levels of CD68. We hypothesized that IC mimicry in tumor cells could attract antigen-presenting cells to elicit immune responses. In this case, the inhibitory immune signals from the CTLA4 immune mimicry further induced macrophage infiltration, contributing to the least permissive TME. Our findings suggest that immune mimicry is a double-edged sword dependent on the type of immune masquerade adopted by the tumor cells. These immune mimicry features provide additional information on the intricacy of the immune landscape within OCCC.

We also noted that tumor samples in the FIGO stage IC1/2 with FN group epithelial cells showed no recurrence, indicating that the phenotype hybrid OCCC with high levels of both PanCK and FN was associated with a better prognosis. However, the FN group tumor cells were relatively cold in immune mimicry, expressed scanty myeloid lineage markers, and did not attract TIIs. Because FN is a well-documented mesenchymal marker, it is interesting that TIIs do not exist within such mesenchymal-like tumor cells. This is consistent with the known immunosuppressive functions elicited using epithelial-mesenchymal transition.[10,34,35]

The immune subtype identified by Ye et al,[25] and the immune-hot subtype identified by Huang et al,[22] both revealed consistently adverse tumor biology related to immune features. However, the bulk analysis in these 2 studies could not delineate whether these immune subtypes were contributed through the infiltration of immune cells or the immune mimicry of tumor cells. The spatially resolved analysis from the current study showed that both the infiltration of immune cells and the immune mimicry of tumor cells play crucial roles in shaping the immune subtype in OCCC.

We identified different combinations of these 5 clusters in OCCC tumors. Intriguingly, epithelial cells with immune-hot features did not exist as stand-alone clusters. The presence of immunomimic tumor cells in tumors with a certain degree of intratumoral heterogeneity suggests that these cells may have been acquired under selection pressure. Our study echoes previous research on the tumor immunoscore,[36-38] suggesting that the immune process is not consistently associated with favorable clinical outcomes and could be either tumor suppressing or tumor promoting. The cluster mixture containing GZMB epithelial cells may be indicative of a tumor-suppressing environment, whereas that containing IL epithelial cells may be tumor promoting.

Our study also highlighted significant changes in specific features associated with early stage OCCC recurrence during tumor progression from FIGO stage IC1/2 to IC3/II (Fig. 5A). Although the spatial profiling data did not allow us to decipher the sequence of switches between tumor and immune cells, we observed a switch in tumor cell clustering related to OCCC recurrence from the IH/IL/IC group to the FN group, indicating a transition from immune-hot mimicry to mesenchymal-like tumor cells. The surrounding immune cells associated with OCCC recurrence showed a cluster switch from the IL group to the IH group, along with a protein expression switch from macrophage lineage TIIs to lymphoid lineage non-TIIs. However, the protein expression levels of immune signals from both TIIs and non-TIIs in IC3/II were similar to those in ICI/2. This indicates that IC3/II tumors are as “hot” as IC1/2 tumors with immune-hot mimicry. We hypothesized that immune-hot mimicry may serve as an indicator of tumor expansion. As OCCC progresses, the TME surrounded by high levels of mesenchymal signals, such as FN and SMA, regulates the immune response and leads to the exclusion of TIIs. This mechanism may strengthen the tumor evasion process, suggesting a poor prognosis. To the best of our knowledge, this is the first study from the spatial profiling aspect to elucidate the interaction between tumor cells and TME during early stage OCCC progression.

In addition, we observed a shift in the morphologic pattern related to OCCC recurrence, from papillary to tubulocystic. Veras et al[15] provided some indirect evidence of the relationship between OCCC morphology and prognosis. They suggested that OCCC could be divided into the following 2 categories: arising from a cyst or from an adenofibroma, which harbors different clinicopathologic factors, including stage at presentation, association with endometriosis, histologic patterns, and survival. Cystic OCCC with a dominant papillary morphology has a better prognosis than adenofibromatous OCCC with a dominant tubulocystic morphology. However, there was still more than 50% OCCC in this study with no predominance of architectural patterns. Instead, these cases displayed a combination of 3 patterns. Similarly, in clear cell renal cell carcinoma, which shares a similar histologic morphology with OCCC, Cai et al[16] defined 33 phenotypes according to spatial architecture, cytologic features, and TME and illustrated their associations with clinical behaviors such as prognosis and drug resistance. After controlling for nucleolar grade and aggressive cytologic features of sarcomatoid/rhabdoid elements, 4 aggressive morphologic patterns—tubular component, chromophobe-renal-cell-carcinoma-like pattern, infiltration into the renal parenchyma, and necrosis—were identified to be predictive of DFS. Both studies suggested that OCCC morphology may be correlated with clinical outcomes, whereas our study further demonstrated that OCCC morphology correlated with the presence of TIIs and clinical outcomes. This may serve as the basis for the future development of an artificial intelligent–driven predictive model for OCCC.

OCCC is recognized for its relative resistance to platinum-based chemotherapy, which may explain its relatively poor prognosis in ovarian carcinoma.[39-41] Consequently, there is an urgent need for novel treatment options for OCCC. Immunotherapy is considered to have potential benefits for patients with OCCC. However, one should be mindful of patient selection because of the limited efficacy observed in the small number of cases.[42,43] Biomarkers predictive of therapeutic efficacy are yet to be identified in case series involving patients with OCCC receiving IC blockade.[44] However, these patients had recurrent or advanced disease and data on their responses to IC blockade in a front-line setting are currently unavailable. Our present study focused on the TME of patients with primary OCCC, and the findings suggest potential biomarkers for patient selection in immunotherapy, including immune-hot features, TIIs, and tumor morphology.

A limitation of this study was its relatively small sample size. In previous studies conducted using DSP, 2 common methods for selecting ROIs have been identified. The first method involves

samples vs the rest, solid patterns but without CD45 segments in FIGO stage IC/II, tubulocystic patterns but without CD45 segments in FIGO stage IC/II, IH group tumor cells and TIIs in FIGO stage IC/II, and IH group tumor cells and papillary patterns in FIGO stage IC1/2, respectively. (D) The 2-year disease-free survival rate of patients with OCCC with specific coexisting features within individual regions of interest (ROIs) vs the rest, papillary patterns and TIIs in FIGO stage IC1/2, and FN group tumor cells and non-TIIs in FIGO stage IC1/2, respectively. DSP, digital spatial profiling; H&E, hematoxylin and eosin; HR, hazard ratio; PanCK, pan-cytokeratin.

Table 2
Univariate analysis of PanCK segments in 22 OCCC tumor samples with specific features.

PanCK	All				IC1/2				IC3/II			
Parameter	n	mDFS (mo)	HR (95% CI)	*P* value	n	mDFS (mo)	HR (95% CI)	*P* value	n	mDFS (mo)	HR (95% CI)	*P* value
GZMB	10	39.7	0.096	0.0012[a]	5	42.3	0.12	0.13	5	37.0	0.083	0.0037[a]
The rest	12	9.2	(0.023-0.40)		5	20.8	(0.0074-1.93)		7	6.3	(0.016-0.45)	
IH	8	12.5	1.43	0.61	4	16.2	15.49	0.062	4	8.5	0.77	0.75
The rest	14	39.7	(0.36-5.60)		6	47.5	(0.87-276.8)		8	22.4	(0.16-3.77)	
IL	1	6.4	1.61	0.71	1	6.4	14.33	0.18	0	-	-	-
The rest	21	19.3	(0.14-18.75)		9	42.3	(0.30-675.4)		12	12.3		
FN	17	19.3	1.03	0.97	6	46.8	0.06	0.062	11	11.9	3.11	0.38
The rest	5	19.3	(0.21-5.05)		4	16.2	(0.0036-1.15)		1	32.0	(0.25-39.43)	
IC	14	37.2	0.38	0.21	9	42.3	3.06	0.63	5	32.0	0.58	0.51
The rest	8	9.2	(0.08-1.74)		1	19.3	(0.034-278.6)		7	6.5	(0.11-2.96)	
Papillary	15	19.3	0.70	0.64	7	20.8	4.33	0.34	8	12.6	0.38	0.28
The rest	7	19.3	(0.15-3.19)		3	42.3	(0.22-85.33)		4	9.1	(0.066-2.21)	
Tubulocystic	18	20.1	0.68	0.67	8	43.0	0.070	0.18	10	9.2	1.83	0.48
The rest	4	16.0	(0.12-3.98)		2	12.9	(0.0015-3.30)		2	22.4	(0.35-9.60)	
Solid	20	20.1	0.42	0.54	9	42.3	0.000045	0.0027[a]	11	12.7	3.05	0.45
The rest	2	9.2	(0.027-6.60)		1	6.4	(6.60e-08-0.031)		1	11.9	(0.17-55.43)	
TII	13	13.1	2.29	0.24	4	17.0	15.49	0.062	9	12.7	0.69	0.69
The rest	9	19.3	(0.57-9.24)		6	43.0	(0.87-276.8)		3	6.5	(0.11-4.30)	
Non-TII	12	16.8	2.95	0.13	3	61.0	0.23	0.34	9	6.5	4.32	0.099
The rest	10	19.3	(0.73-11.84)		7	19.3	(0.012-4.56)		3	13.3	(0.76-24.50)	
No CD45	15	19.3	0.26	0.10	10	31.6	-	-	5	12.7	0.58	0.50
The rest	7	6.5	(0.052-1.29)		0	-			7	6.5	(0.12-2.88)	

FN, fibronectin; GZMB, granzyme B; HR, hazard ratio; IC, immune checkpoint; IH, immune signal high; IL, immune like; mDFS, median disease-free survival; OCCC, ovarian clear cell carcinoma; PanCK, pan-cytokeratin; TIIs, tumor-infiltrating immune cells.
[a] The value with significance.

choosing a higher number of patients but a lower number of ROIs in each patient sample,[45] allowing for a focus on high intertumoral heterogeneity, but potentially overlooking intratumoral heterogeneity. This approach may be suitable for homogeneous or small tumors. The second method involves selecting a lower number of patients but a higher number of ROIs in each patient sample,[46] providing a more comprehensive exploration of intratumoral heterogeneity. Because of the complex morphology and large size

Table 3
Univariate analysis of CD45 segments in 22 OCCC tumor samples with specific features.

CD45	All				IC1/2				IC3/II			
Parameter	n	mDFS (mo)	HR (95% CI)	*P* value	n	mDFS (mo)	HR (95% CI)	*P* value	n	mDFS (mo)	HR (95% CI)	*P* value
GZMB	2	46.5	0.30	0.15	1	61.0	0.30	0.38	1	32.0	0.31	0.27
The rest	20	16.3	(0.059-1.57)		9	20.8	(0.019-4.54)		11	11.9	(0.036-2.56)	
IH	10	9.2	6.16	0.0029[a]	4	16.2	16.75	0.0068[a]	6	5.9	5.06	0.045[a]
The rest	12	43.0	(1.86-20.40)		6	47.5	(2.18-128.9)		6	24.5	(1.04-24.63)	
IL	15	19.3	1.09	0.89	7	20.8	1.97	0.49	8	13.0	1.34	0.71
The rest	7	19.3	(0.34-3.52)		3	42.3	(0.29-13.27)		4	9.2	(0.29-6.27)	
FN	3	43.7	0.55	0.45	2	55.4	0.24	0.18	1	5.4	7.11	0.27
The rest	19	19.3	(0.12-2.60)		8	20.1	(0.029-1.94)		11	12.7	(0.22-228.5)	
IC	10	34.5	0.36	0.077	4	40.9	0.92	0.93	6	34.5	0.13	0.0112[a]
The rest	12	13.1	(0.12-1.12)		6	30.8	(0.15-5.78)		6	6.4	(0.026-0.63)	
Papillary	12	17.1	1.04	0.94	5	20.8	2.02	0.45	7	13.3	0.60	0.56
The rest	10	19.3	(0.35-3.14)		5	42.3	(0.32-12.55)		5	6.5	(0.16-2.75)	
Tubulocystic	13	20.8	0.72	0.56	5	43.7	0.42	0.36	7	12.6	0.91	0.90
The rest	9	13.1	(0.23-2.23)		5	19.3	(0.066-2.68)		5	9.6	(0.21-3.98)	
Solid	13	20.8	0.61	0.32	4	40.9	0.92	0.93	9	12.7	0.46	0.36
The rest	9	19.3	(0.23-1.61)		6	30.8	(0.15-5.78)		3	11.9	(0.084-2.48)	
TII	14	17.0	0.80	0.69	5	20.8	1.66	0.46	9	12.7	0.40	0.30
The rest	8	19.3	(0.26-2.45)		5	42.3	(0.43-6.40)		3	6.5	(0.072-2.26)	
Non-TII	14	16.3	1.04	0.95	4	40.9	2.02	0.45	10	12.3	1.67	0.56
The rest	8	25.7	(0.34-3.21)		6	30.8	(0.32-12.55)		2	19.3	(0.29-9.58)	

FN, fibronectin; GZMB, granzyme B; HR, hazard ratio; IC, immune checkpoint; IH, immune signal high; IL, immune like; mDFS, median disease-free survival; OCCC, ovarian clear cell carcinoma; TIIs, tumor-infiltrating immune cells.
[a] The value with significance.

of OCCC tumors, we opted for the latter selection method to thoroughly examine each tumor sample. Another major limitation comes from DSP technology itself. Single-cell resolution is needed for the absolute confirmation that each tumor cell expresses immune signals, whereas the default design of the DSP platform did not provide such profiling resolution down to single-cell levels. At the time we conducted this study, single-cell based spatial omics technology was yet to be commercially available.[47] Therefore, further exploration using single-cell spatial transcriptomics platforms is highly mandated. Nevertheless, other studies also have similar findings that certain immune features were differentially expressed in the PanCK+ epithelial segments at the protein level.[19,48] This suggests that segmentation performance could be rather robust and there might truly exist a universal "immune mimicry" phenomenon. The interaction between the immune mimicry of tumor cells and TIIs could be a complex issue. Further investigation with a larger sample size and single-cell resolution is warranted.

Acknowledgments

This work was supported by the Yushan Scholar Program of the Ministry of Education, Taiwan (NTU-112V1402-5), and National Taiwan University Core Consortium (NTUCC-112L894903) to R.Y.-J.H., and NTUCC-112L894901 to L.-H.W.

Author Contributions

R.Y.-J.H. and L.-H.W. conceptualized the study. D.Y.-T.W., Y.-T.T., W.-C.L., and R.Y.-J.H. wrote the manuscript. Y.-T.T., J.Y., D.Y.-T.W., D.T.-H.C., and K.-C.C. performed digital spatial profiling data acquisition. Y.-T.T., D.Y.-T.W., and T.Z.T. performed data analysis and interpretation. W.-C.L. performed pathology review. L.-H.W. and Y.-T.T. performed clinical review. All the authors have read and agreed to the final version of the manuscript.

Data Availability

The data that support the findings of this study are available from the authors.

Funding

This work was supported by the Yushan Scholar Program of the Ministry of Education, Taiwan (NTU-112V1402-5), and National Taiwan University Core Consortium (NTUCC-112L894903) to R.Y.-J.H., and NTUCC-112L894901 to L.-H.W.

Declaration of Competing Interest

The authors declare no conflict of interest.

Ethics Approval and Consent to Participate

This study was approved by the Institutional Review Board of National Taiwan University Hospital (reference number: 20200508RIND), which waived the need for informed consent.

Supplementary Material

The online version contains supplementary material available at https://doi.org/10.1016/j.modpat.2024.100630

References

1. Siegel RL, Miller KD, Wagle NS, Jemal A. Cancer statistics, 2023. *CA Cancer J Clin*. 2023;73(1):17–48.
2. Prat J, D'Angelo E, Espinosa I. Ovarian carcinomas: at least five different diseases with distinct histological features and molecular genetics. *Hum Pathol*. 2018;80:11–27.
3. McCluggage WG. Morphological subtypes of ovarian carcinoma: a review with emphasis on new developments and pathogenesis. *Pathology*. 2011;43(5):420–432.
4. Zhu C, Xu Z, Zhang T, et al. Updates of pathogenesis, diagnostic and therapeutic perspectives for ovarian clear cell carcinoma. *J Cancer*. 2021;12(8):2295–2316.
5. Tan DSP, Iravani M, McCluggage WG, et al. Genomic analysis reveals the molecular heterogeneity of ovarian clear cell carcinomas. *Clin Cancer Res*. 2011;17(6):1521–1534.
6. Yin X, Bi R, Ma P, et al. Multiregion whole-genome sequencing depicts intratumour heterogeneity and punctuated evolution in ovarian clear cell carcinoma. *J Med Genet*. 2020;57(9):605–609.
7. Wiegand KC, Shah SP, Al-Agha OM, et al. ARID1A mutations in endometriosis-associated ovarian carcinomas. *N Engl J Med*. 2010;363(16):1532–1543.
8. Yamamoto S, Tsuda H, Takano M, Iwaya K, Tamai S, Matsubara O. PIK3CA mutation is an early event in the development of endometriosis-associated ovarian clear cell adenocarcinoma. *J Pathol*. 2011;225(2):189–194.
9. Heong V, Tan TZ, Miwa M, et al. A multi-ethnic analysis of immune-related gene expression signatures in patients with ovarian clear cell carcinoma. *J Pathol*. 2021;255(3):285–295.
10. Tan TZ, Ye J, Yee CV, et al. Analysis of gene expression signatures identifies prognostic and functionally distinct ovarian clear cell carcinoma subtypes. *EBioMedicine*. 2019;50:203–210.
11. Okamoto A, Glasspool RM, Mabuchi S, et al. Gynecologic Cancer InterGroup (GCIG) consensus review for clear cell carcinoma of the ovary. *Int J Gynecol Cancer*. 2014;24(9 suppl 3):S20–S25.
12. Hendry S, Salgado R, Gevaert T, et al. Assessing tumor infiltrating lymphocytes in solid tumors: a practical review for pathologists and proposal for a standardized method from the International Immuno-Oncology Biomarkers Working Group: part 2: TILs in melanoma, gastrointestinal tract carcinomas, non-small cell lung carcinoma and mesothelioma, endometrial and ovarian carcinomas, squamous cell carcinoma of the head and neck, genitourinary carcinomas, and primary brain tumors. *Adv Anat Pathol*. 2017;24(6):311–335.
13. Zhang L, Conejo-Garcia JR, Katsaros D, et al. Intratumoral T cells, recurrence, and survival in epithelial ovarian cancer. *N Engl J Med*. 2003;348(3):203–213.
14. Santoiemma PP, Powell Jr DJ. Tumor infiltrating lymphocytes in ovarian cancer. *Cancer Biol Ther*. 2015;16(6):807–820.
15. Veras E, Mao T-L, Ayhan A, et al. Cystic and adenofibromatous clear cell carcinomas of the ovary: distinctive tumors that differ in their pathogenesis and behavior: a clinicopathologic analysis of 122 cases. *Am J Surg Pathol*. 2009;33(6):844–853.
16. Cai Q, Christie A, Rajaram S, et al. Ontological analyses reveal clinically-significant clear cell renal cell carcinoma subtypes with convergent evolutionary trajectories into an aggressive type. *EBioMedicine*. 2020;51:102526.
17. DeLair D, Oliva E, Köbel M, Macias A, Gilks CB, Soslow RA. Morphologic spectrum of immunohistochemically characterized clear cell carcinoma of the ovary: a study of 155 cases. *Am J Surg Pathol*. 2011;35(1):36–44.
18. Ju B, Wang J, Yang B, et al. Morphologic and immunohistochemical study of clear cell carcinoma of the uterine endometrium and cervix in comparison to ovarian clear cell carcinoma. *Int J Gynecol Pathol*. 2018;37(4):388–396.
19. Merritt CR, Ong GT, Church SE, et al. Multiplex digital spatial profiling of proteins and RNA in fixed tissue. *Nat Biotechnol*. 2020;38(5):586–599.
20. Beechem JM. High-plex spatially resolved RNA and protein detection using digital spatial profiling: a technology designed for immuno-oncology biomarker discovery and translational research. *Methods Mol Biol*. 2020;2055:563–583.
21. Van TM, Blank CU. A user's perspective on GeoMxTM digital spatial profiling. *Immunooncol Technol*. 2019;1:11–18.
22. Huang RYJ, Huang KJ, Chen KC, et al. Immune-hot tumor features associated with recurrence in early-stage ovarian clear cell carcinoma. *Int J Cancer*. 2023;152(10):2174–2185.
23. Eisen M. *Cluster 3.0 Manual*. 2024. Accessed November 6, 2024. http://bonsai.hgc.jp/~mdehoon/software/cluster/cluster3.pdf
24. Saldanha AJ. Java Treeview–extensible visualization of microarray data. *Bioinformatics*. 2004;20(17):3246–3248.
25. Ye S, Li Q, Wu Y, et al. Integrative genomic and transcriptomic analysis reveals immune subtypes and prognostic markers in ovarian clear cell carcinoma. *Br J Cancer*. 2022;126(8):1215–1223.
26. Tímár J, Honn KV, Hendrix MJC, Marko-Varga G, Jalkanen S. Newly identified form of phenotypic plasticity of cancer: immunogenic mimicry. *Cancer Metastasis Rev*. 2023;42(1):323–334.
27. Frangieh CJ, Melms JC, Thakore PI, et al. Multimodal pooled Perturb-CITE-seq screens in patient models define mechanisms of cancer immune evasion. *Nat Genet*. 2021;53(3):332–341.

28. Thorsson V, Gibbs DL, Brown SD, et al. The immune landscape of cancer. *Immunity*. 2018;48(4):812–830.e14.
29. Gao R, He B, Huang Q, et al. Cancer cell immune mimicry delineates onco-immunologic modulation. *iScience*. 2021;24(10):103133.
30. Al-Shibli KI, Donnem T, Al-Saad S, Persson M, Bremnes RM, Busund L-T. Prognostic effect of epithelial and stromal lymphocyte infiltration in non–small cell lung cancer. *Clin Cancer Res*. 2008;14(16):5220–5227.
31. Nedergaard BS, Ladekarl M, Nyengaard JR, Nielsen K. A comparative study of the cellular immune response in patients with stage IB cervical squamous cell carcinoma. Low numbers of several immune cell subtypes are strongly associated with relapse of disease within 5 years. *Gynecol Oncol*. 2008;108(1):106–111.
32. Schmidt M, Böhm D, von Törne C, et al. The humoral immune system has a key prognostic impact in node-negative breast cancer. *Cancer Res*. 2008;68(13):5405–5413.
33. Nielsen JS, Sahota RA, Milne K, et al. $CD20^{+}$ tumor-infiltrating lymphocytes have an atypical $CD27^{-}$ memory phenotype and together with $CD8^{+}$ T cells promote favorable prognosis in ovarian cancer. *Clin Cancer Res*. 2012;18(12):3281–3292.
34. Terry S, Savagner P, Ortiz-Cuaran S, et al. New insights into the role of EMT in tumor immune escape. *Mol Oncol*. 2017;11(7):824–846.
35. Akalay I, Janji B, Hasmim M, et al. Epithelial-to-mesenchymal transition and autophagy induction in breast carcinoma promote escape from T-cell–mediated lysis. *Cancer Res*. 2013;73(8):2418–2427.
36. Bruni D, Angell HK, Galon J. The immune contexture and Immunoscore in cancer prognosis and therapeutic efficacy. *Nat Rev Cancer*. 2020;20(11):662–680.
37. Galon J, Mlecnik B, Bindea G, et al. Towards the introduction of the 'Immunoscore'in the classification of malignant tumours. *J Pathol*. 2014;232(2):199–209.
38. Galon J, Pagès F, Marincola FM, et al. Cancer classification using the Immunoscore: a worldwide task force. *J Transl Med*. 2012;10:205.
39. Pectasides D, Pectasides E, Psyrri A, Economopoulos T. Treatment issues in clear cell carcinoma of the ovary: a different entity? *Oncologist*. 2006;11(10):1089–1094.
40. Pectasides D, Fountzilas G, Aravantinos G, et al. Advanced stage clear-cell epithelial ovarian cancer: the Hellenic Cooperative Oncology Group experience. *Gynecol Oncol*. 2006;102(2):285–291.
41. Gorai I, Nakazawa T, Miyagi E, Hirahara F, Nagashima Y, Minaguchi H. Establishment and characterization of two human ovarian clear cell adenocarcinoma lines from metastatic lesions with different properties. *Gynecol Oncol*. 1995;57(1):33–46.
42. Signorelli D, Giannatempo P, Grazia G, et al. Patients selection for immunotherapy in solid tumors: overcome the naïve vision of a single biomarker. *BioMed Res Int*. 2019;2019:9056417.
43. Copier J, Dalgleish AG, Britten CM, et al. Improving the efficacy of cancer immunotherapy. *Eur J Cancer*. 2009;45(8):1424–1431.
44. Sia TY, Manning-Geist B, Gordhandas S, et al. Treatment of ovarian clear cell carcinoma with immune checkpoint blockade: a case series. *Int J Gynecol Cancer*. 2022;32(8):1017–1024.
45. Martinez-Morilla S, Moutafi M, Fernandez AI, et al. Digital spatial profiling of melanoma shows CD95 expression in immune cells is associated with resistance to immunotherapy. *Oncoimmunology*. 2023;12(1):2260618.
46. Schneider F, Kaczorowski A, Jurcic C, et al. Digital spatial profiling identifies the tumor periphery as a highly active biological niche in clear cell renal cell carcinoma. *Cancers (Basel)*. 2023;15(20):5050.
47. Hernandez S, Lazcano R, Serrano A, et al. Challenges and opportunities for immunoprofiling using a spatial high-plex technology: the NanoString GeoMx® digital spatial profiler. *Front Oncol*. 2022;12:890410.
48. Qurat-Ul-Ain, Frei NF, Khoshiwal AM, et al. Feasibility study utilizing NanoString's digital spatial profiling (DSP) technology for characterizing the immune microenvironment in Barrett's esophagus formalin-fixed paraffin-embedded tissues. *Cancers (Basel)*. 2023;15(24):5895.